

Pale Cytochrome Oxidase Stripes in V2 Receive the Richest Projection From Macaque Striate Cortex

LAWRENCE C. SINCICH* AND JONATHAN C. HORTON

Beckman Vision Center, University of California, San Francisco, San Francisco, California 94143

ABSTRACT

Once the visual pathway reaches striate cortex, it fans out to a number of extrastriate areas. The projections to the second visual area (V2) are known to terminate in a patchy manner. V2 contains a system of repeating pale-thin-pale-thick stripes of cytochrome oxidase (CO) activity. We examined whether the patchy terminal fields arising from primary visual cortex (V1) projections are systematically related to the CO stripes in V2. Large injections of an anterograde tracer, [³H]proline, were made into V1 of both hemispheres in 5 macaques. The resulting V2 label appeared in layers 2–6, with the densest concentration in layer 4. In 21/29 injections, comparison of adjacent flatmount sections processed either for autoradiography or CO activity showed that the heaviest [³H]proline labeling was located in pale CO stripes. In 7/29 injections, there was no clear enrichment of labeling in the CO pale stripes. In 1 injection, the proline label correlated with dark CO stripes. On a fine scale, CO levels vary within V2 stripes, giving them an irregular, mottled appearance. In all stripe types, the density of proline label would often wax and wane in opposing contrast to these local fluctuations in CO density. Our data showed that V1 input is generally anti-correlated with the intensity of CO staining in V2, with strongest input to pale stripes. It is known that the pulvinar projects preferentially to dark stripes. Therefore, V2 receives interleaved projections from V1 and the pulvinar. Because these projections favor different stripe types, they may target separate populations of neurons. *J. Comp. Neurol.* 447: 18–33, 2002. © 2002 Wiley-Liss, Inc.

Indexing terms: visual cortex; pulvinar; extrastriate cortex; cortical columns; intracortical projections; flatmount

In primates, the main pathway serving visual perception flows from the retina via the lateral geniculate body to the primary (striate, V1) visual cortex. Visual information is then conveyed to the second visual area (V2), before dissemination to higher visual areas. Although direct projections exist from V1 to areas V3 and middle temporal area (MT) or (V5), the major link between striate and extrastriate cortex is provided by the connections from V1 to V2 (Poliak, 1932, p. 206; Mettler, 1935; Kuypers et al., 1965; Cragg, 1969; Zeki, 1969; Rockland and Pandya, 1979; Lund et al., 1981). Delineating the anatomy of this projection is crucial for understanding how visual information is processed in the primate brain.

V1 and V2 share a common border, containing the representation of the vertical meridian. Consequently, injection of an anterograde tracer into V1 results in label at a mirror image location in V2. Wong-Riley (1979b) showed, curiously, that single tracer injections into V1 always produce multiple bands of label in V2. She described “labelled columns (120–480 μm in diameter, commonly 240

μm) interdigitating with sparsely labelled or unlabelled columns of lesser widths.” Her observations have been confirmed by many investigators (Martinez-Millán and Holländer, 1975; Rockland and Pandya, 1979; Maunsell et al., 1980; Lund et al., 1981; Weller and Kaas, 1983; Van Essen et al., 1986). The reason for this patchy input to V2 has never been explained.

Grant sponsor: National Eye Institute; Grant numbers: R01-EY10217, F32-EY13676, P30-EY02162; Grant sponsor: That Man May See, Inc.; Grant sponsor: Research to Prevent Blindness.

*Correspondence to: Lawrence C. Sincich, Ph.D., Beckman Vision Center, University of California, San Francisco, 10 Koret Way, San Francisco, CA 94143-0730. E-mail: sincich@itsa.ucsf.edu

Received 26 September 2001; Revised 14 December 2001; Accepted 2 January 2002

DOI 10.1002/cne.10179

Published online the week of April 1, 2002 in Wiley InterScience (www.interscience.wiley.com).

In macaques and humans, area V2 contains a system of coarse bands of alternating light and dark cytochrome oxidase (CO) activity, oriented perpendicular to the V1/V2 border (Horton, 1984). In the squirrel monkey, Tootell et al. (1983) recognized that there are two distinct types of dark stripes: thick and thin. Thus, V2 forms a corona of repeating pale-thin-pale-thick stripes encircling V1. Although this tripartite pattern of stripes is less readily visualized in macaques (Livingstone and Hubel, 1984; Tootell and Hamilton, 1989; Crawford and Chodosh, 1990), it can be easily identified in flatmounted tissue (Olavarria and Van Essen, 1997). Surprisingly, it is unknown whether the CO stripes in V2 bear any relationship to the patchy terminal fields seen after anterograde tracer injection in V1.

A regular relationship might be expected, because afferent input to a given cortical area often governs its CO levels. In V1, for example, the laminar pattern of CO staining matches the distribution of transneuronal label seen after a [³H]proline injection into the eye (Horton, 1984). CO activity is especially rich in layers 6, 4C, and 4A, which are precisely the layers that receive direct input from the parvo and magno layers of the lateral geniculate body. In tangential sections, there is a perfect coincidence between each puff of geniculate label in layer 3 and the location of the CO patches (Livingstone and Hubel, 1982; Horton, 1984; Hendry and Yoshioka, 1994; Ding and Casagrande, 1997). The lesson from V1 is that the pattern of baseline metabolic activity, at least in terms of CO levels, corresponds to the major source of ascending thalamic input.

The goal of this present study was to determine whether the bands of V1 input discovered by Wong-Riley might be related to the pale-thin-pale-thick stripes of CO activity in V2. Based on the precedent in V1, it would be expected that the dark CO stripes, being more active metabolically, would receive stronger input. To test this idea, we made large injections of an anterograde tracer, [³H]proline, into macaque V1 and compared the resulting bands of label with the CO stripes in V2.

MATERIALS AND METHODS

Experimental animals and surgical procedures

Five *Macaca mulatta* monkeys weighing between 2.8 and 3.8 kg from the California Regional Primate Research Center (Davis, CA) were used. The experiments were approved by the UCSF Committee on Animal Research. A total of 34 injections of [³H]proline were made. In four monkeys we made 3 tracer injections in dorsal V1 of each hemisphere. In one animal, 2 additional injections were made in ventral V1 of each hemisphere (Table 1).

Proline was selected as a tracer because it yields strong anterograde labeling, with little contamination from retrograde uptake. We also favored proline because it was the tracer used by previous investigators to demonstrate patchy projections from V1 to V2 (Rockland and Pandya, 1979; Wong-Riley, 1979b; Weller and Kaas, 1983; Van Essen et al., 1986). Three days after proline injection, the majority of label is concentrated in synaptic terminals (Hendrickson, 1972). Therefore, autoradiographic labeling in the cortex provides a reliable index of synaptic density, although we did not analyze tissue at the ultrastructural level.

General anesthesia was induced with ketamine HCl (10 mg/kg, i.m.). The animal was intubated endotracheally and anesthesia was maintained with 2% isoflurane in a 1:1 mixture of N₂O:O₂. During the experiment, we monitored the EKG, respiratory rate, body temperature, blood oxygenation (SpO₂), endtidal CO₂, and inspired/expired levels of anesthetic gases. A 5% dextrose in half-normal saline solution was delivered intravenously at 3–4 ml/kg/hour. After the animal was placed in a stereotaxic frame, a craniotomy was performed over dorsal V1 and the lunate sulcus. A U-shaped durotomy was made to expose the dorsal operculum for tracer injections.

The anterograde tracer was prepared by reconstituting 0.25–1.0 mCi of L-[2,3,4,5-³H]proline (specific activity 99.0 Ci/mmol; Amersham, Arlington Heights, IL) in sterile balanced salt solution. The solution was filtered through 0.2 μm pores. Injections varied between 15 and 100 μCi. They were delivered in 140–280 nl of balanced salt solution. A beveled glass micropipette (15 μm inner diameter) was front-filled with sufficient tracer to make all of the injections during one experiment. The injections were placed in V1 5–10 mm posterior to the lunate sulcus, about 10 mm apart in the mediolateral direction, to produce labeling in dorsal V2 along the posterior bank of the lunate sulcus. Injections were placed at a cortical depth of ~500 μm, targeting the base of layer 3. The tracer was injected by pressure over 3–5 minutes. After the injections were completed, the dura was closed with 8-0 nylon suture, and the bone flap was glued back in place. The entire procedure was repeated in the other hemisphere. Buprenorphine (0.02 mg/kg i.m.) was given postoperatively for analgesia every 8 hours until the animal showed no signs of discomfort.

Histological procedures

After allowing 4–8 days for transport, the animals were given a lethal dose of sodium pentobarbital (150 mg/kg) and cardially perfused with 1 L of 0.9% saline followed by 1 liter of 1% paraformaldehyde in 0.1 M phosphate buffer (PB), pH 7.4. The brain was removed and flatmounts were prepared containing opercular V1, V2, and surrounding extrastriate areas (Olavarria and Van Sluysters, 1985; Tootell and Silverman, 1985). The flatmounts were left overnight in 1.33% paraformaldehyde plus 30% sucrose in PB at room temperature under light pressure (~4 g/cm²). The weight was then removed and the tissue was transferred to 4°C for an additional 24 hours.

Frozen sections were cut parallel to the pial surface at 40 μm for CO sections and 30 or 40 μm for autoradiographic sections. In Monkey 1, alternating sections were processed for autoradiography or CO. In the remaining animals, most of the sections were reacted for CO (Wong-Riley, 1979a; Horton, 1984), with occasional, interspersed sections consigned to autoradiography. In every animal, some double-label sections were reacted for CO, analyzed, photographed, and subsequently dipped for autoradiography (Horton and Hocking, 1996).

In the single animal with ventral V1 injections, we removed an intact block of tissue containing the inferior occipital sulcus from the left hemisphere prior to flattening. This block was sunk in 1% paraformaldehyde plus 30% sucrose in PB at 4°C. Horizontal sections were cut at 50 μm, mounted on slides in a one-in-three series, and processed for either autoradiography, CO, or Nissl substance.

Data analysis

Digital photographs of the sections were made with a cooled, SPOT RT color CCD camera (Diagnostic Instruments, Sterling Heights, MI) mounted on an Olympus SZH10 microscope. Some photographs were taken with a Nikon 55 mm macro lens attached to the CCD camera. All photographic exposures were made to span but not exceed the 8-bit mode of the camera. The autoradiographic images were photographed with darkfield illumination for maximum contrast, and then digitally inverted to facilitate comparison with CO sections.

Contour plots of the [^3H]proline label were made by processing images in Matlab (Mathworks, Natick, MA). The images were convolved with a gaussian kernel ($\sigma_{1/2} = 50 \mu\text{m}$) to generate smoother contour profiles. The contour profiles were made by dividing the range of grayscale values in each image into 9 equal levels. This yielded a set of 8 contour lines which linearly depicted relative silver grain density. The contour lines were gray-coded so that white and black represented the lowest and highest grain densities, respectively. The contour plots were not normalized or calibrated (except as indicated in Fig. 8). Therefore, they do not represent absolute values of grain density. For illustration purposes only, the brightness and contrast of images were adjusted in Photoshop 6.0 (Adobe Systems, San Jose, CA).

Grayscale images of CO sections were derived from the "green" values of the original RGB photograph (these values have the highest contrast among the three scans used to produce a color image). Global adjustments were made in contrast and brightness to enhance the visibility of CO patterns.

Autoradiographic labeling was compared to CO staining in adjacent sections by superimposing the contour plots on the CO sections. Blood vessel profiles in the autoradiographs and CO sections were used for alignment. For image alignment, only rotation and translation of the images was performed; no scaling or warping was used.

To classify the relationship between the autoradiographic label and CO activity, each injection was rated in the following manner. The peak density of autoradiographic label was identified by the darkest contour profile. If it coincided with a dark (either thin or thick) CO stripe, the [^3H]proline label was considered to be "correlated" with CO activity. If the peak density of [^3H]proline label fell cleanly on a pale CO stripe, it was counted as "anti-correlated." If the peak of proline label density straddled or crossed stripe boundaries, it was considered "uncorrelated." There were usually multiple peaks of label density in the V2 projection field arising from each V1 proline injection. A peak was defined as independent if it was separated from the main peak by a saddle of at least 2 contour levels. To be rated as "correlated," all the proline peaks in a given projection field had to coincide with dark CO stripes. To be rated "anti-correlated," all the peaks had to land on pale CO stripes. If the peaks hit pale and dark CO stripes, they were classified as "uncorrelated." Categorization of the terminal fields was performed independently by each author, and by two observers unrelated to the project.

Alternatively, the data could have been analyzed by correlating the grayscale values in the CO images on a pixel-by-pixel basis with the grayscale values in the autoradiographs. We performed this analysis for several pro-

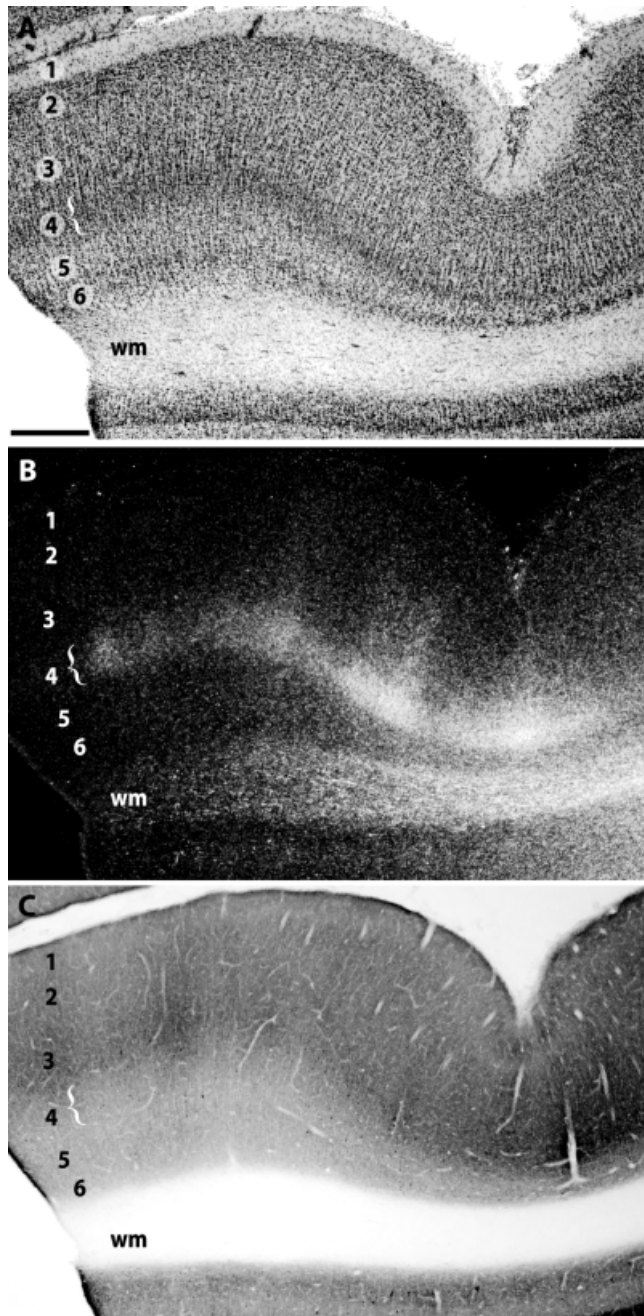


Fig. 1. Monkey 1, left hemisphere. **A:** Nissl-stained section through second visual area (V2) showing the cortical layers. The section was cut horizontally through the posterior bank of the inferior occipital sulcus in the single animal which received ventral primary visual cortex (V1) proline injections. The plane of section was not quite perpendicular to the pial surface. Layers are indicated by numbers and wm denotes white matter. **B:** Darkfield autoradiograph of an adjacent section, showing patchy, dense label in layer 4, with weaker label extending into other layers. **C:** Adjacent section reacted for cytochrome oxidase (CO). The darkest CO staining appeared in layer 3, and did not coincide with the densest band of proline input to layer 4 (compare brackets). Scale bars = 0.5 mm for A–C.

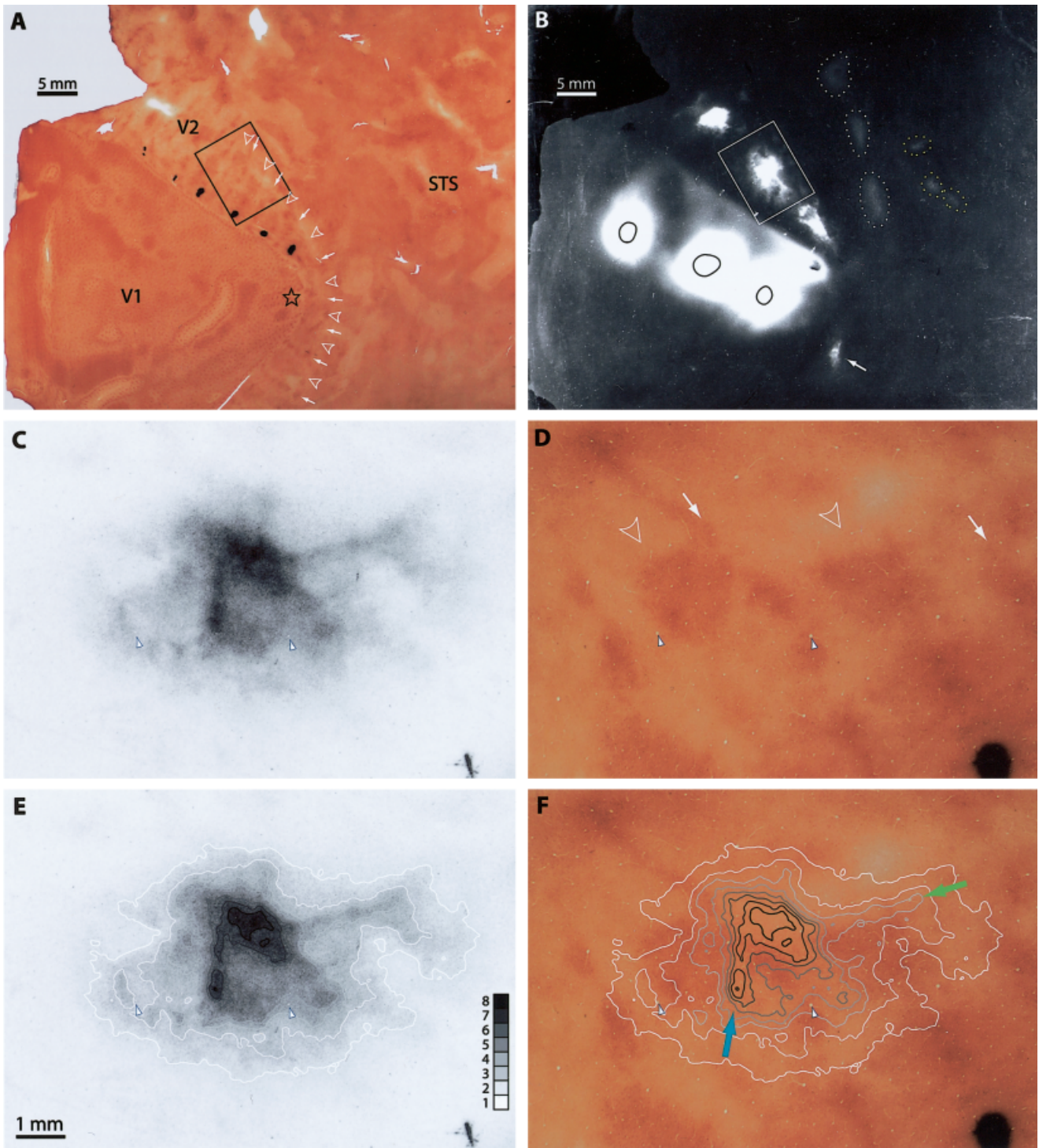


Fig. 2. Monkey 2, right hemisphere. **A:** Single flatmount section of primary visual cortex (V1) and extrastriate cortex reacted for cytochrome oxidase (CO). The star denotes the foveal representation in V1. The left edge of the section is medial, where the right hemisphere folds into the calcarine sulcus. Second visual area (V2) is visible as a cycle of pale-thin-pale-thick CO stripes. Thin stripes are indicated by arrows and thick stripes by open arrowheads. STS indicates the superior temporal sulcus. Area enclosed by the black rectangle in V2 is shown at higher magnification in D and F. The string of 6 tiny, black tracer injections in V2 close to the V1 border pertain to a separate study, reported elsewhere (Sincich and Horton, 2002). **B:** Darkfield autoradiograph of a section adjacent to A, exposed to show to best advantage the anterograde projection fields in extrastriate cortex resulting from three [^3H]proline injections in V1 (centers marked by black ovoids). In dorsal V2, three areas of [^3H]proline label, mirror images of the corresponding V1 injections, are visible. In addition, a field of label is apparent in ventral V2 (arrow) arising from

the foveal-most injection which crossed into ventral V1. A triplet of large, faintly labeled fields (white dotted outlines) was seen in the crown of the prelunate gyrus, possibly corresponding to area V3, V3A, or V4. A smaller triplet of labeled fields (yellow dotted outlines) was present in the STS, presumably in the middle temporal area (MT). The white rectangle, matching in location the black rectangle in A, outlines the fields shown at higher magnification in C and E. **C:** Gray-scale-inverted image of patchy V2 [^3H]proline label, with prominent blood vessels marked with arrowheads. **D:** Matching field of CO activity, with thick (open arrowheads) and thin (arrows) stripes separated by pale stripes. Blood vessels used for alignment with C are marked with arrowheads in D-F. **E:** Contour plot of the density of [^3H]proline label superimposed on the original image in C. There were two peaks in proline intensity. **F:** Contour plot of the proline label in C, transferred onto the CO section in D. In this overlay, the two peaks of [^3H]proline label are positioned over pale CO stripes. Colored arrows are described in text. Scale bars = 5 mm for A-B, 1 mm for C-F.

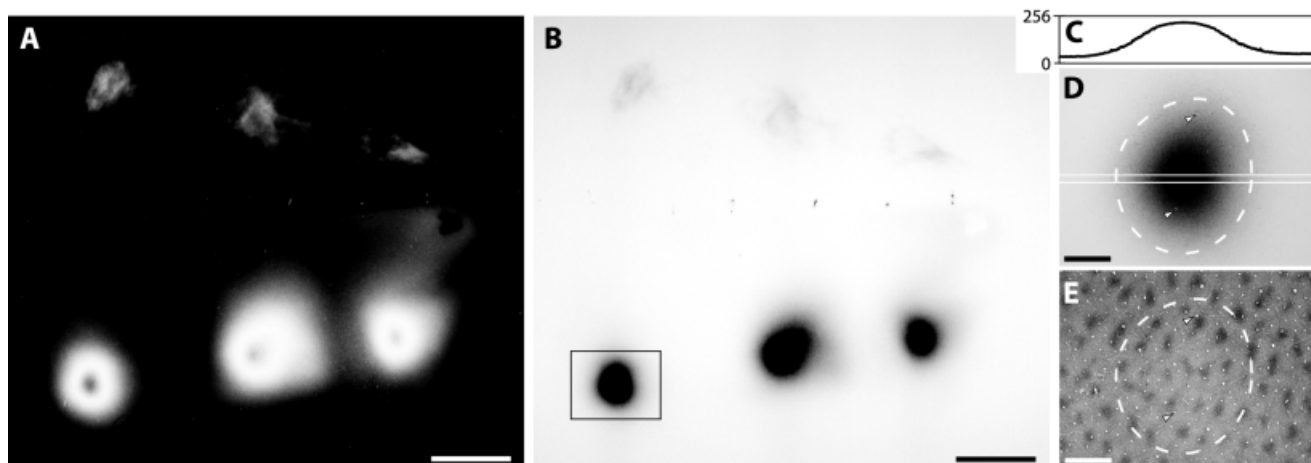


Fig. 3. **A:** Darkfield image of Figure 2B taken with a shorter exposure. The three injections are clearly discrete with this exposure. **B:** Photograph of the same section, taken in brightfield, with an exposure that spans the 8-bit range of the CCD camera. (in all other figures, darkfield pictures have been digitally inverted to achieve a brightfield effect). **C:** Plot of the grayscale values measured through the middle of the injection outlined in B. **D:** Field outlined with the black rectangle in B. The white lines bracket the strip used to plot the grayscale values in C. Dashed outline encircles the field of labeled cell

bodies which have taken up [^3H]proline (not visible at this magnification). These labeled cells provide an indication of the effective uptake zone. **E:** Cytochrome oxidase (CO) section from layer 2/3 at the injection site shown in D. The dashed outline contains roughly 20 CO patches. The darkest part of the injection (which is nearly flat in the density plot above) covers many CO patches and interpatches. Note that the injection itself caused no lesion in the tissue. Arrowheads show blood vessel profiles used for section alignment. Scale bars = 5 mm for A,B, 1 mm for D,E.

jection fields and obtained correlation coefficients that confirmed the analysis obtained by subjectively rating the CO stripes as pale, thin, or thick. However, this approach was less useful because spatial information was lost concerning the relationship between patterns formed by the 2 labels.

RESULTS

Figure 1A shows a Nissl-stained cross-section through area V2. An adjacent section (Figure 1B) shows the distribution of autoradiographic label arising from a single injection of [^3H]proline in V1. Comparison with the Nissl-stained section shows that layer 4 receives the heaviest concentration of label, but weaker label extends into layers 2/3, 5, and 6 (Martinez-Millán and Holländer, 1975; Rockland and Pandya, 1979; Wong-Riley, 1979b; Lund et al., 1981; Weller and Kaas, 1983; Van Essen et al., 1986; Rockland and Virga, 1990). An adjacent section reacted for CO (Fig. 1C) shows that the darkest staining is found in layer 3, just above the heaviest tier of [^3H]proline label. This discordance between the proline label and CO shows that in V2, the strongest metabolic activity does not coincide with maximum V1 input, at least in terms of cortical layers.

As shown by Wong-Riley (1979b), the proline label in V2 fluctuated in density, even though it arose from a single injection in V1. It is difficult to reconstruct the pattern formed by terminal labeling in V2 by examining cortical cross-sections. A far better approach is to physically unfold and flatten the tissue before sectioning to prepare flatmounts of the cortex. Such preparations afford a bird's eye view of the pattern of label throughout the flattened cortex. In addition, one can see the CO pattern of pale-thin-pale-thick stripes to best advantage. Finally, only in flatmounts can blood vessels be used reliably for precise

alignment of adjacent sections to compare patterns of proline and CO.

Figure 2A shows a single flattened section, stained for CO, containing opercular V1, a surrounding belt of V2, and neighboring extrastriate cortex. The pale, thin, and thick stripes in V2 can be easily differentiated. An adjacent autoradiograph, photographed with darkfield illumination, is shown in Figure 2B. The three V1 proline injections yielded three triplets of anterograde labeling in dorsal extrastriate cortex. The most abundant labeling was found in V2, a clear sign that among cortical areas it receives the majority of V1's output.

Beyond V2, three faint patches of label were seen in another visual area, perhaps corresponding to area V3, V3A, V4, DM, DI, or DL (Cragg, 1969; Zeki, 1969, 1978; Van Essen and Zeki, 1978; Burkhalter et al., 1986; Van Essen et al., 1986; Gattass et al., 1988; Felleman et al., 1997; Beck and Kaas, 1999). There is no consensus in the literature regarding the names and boundaries of these extrastriate areas. In the superior temporal sulcus, three closely spaced patches of label were visible. This projection was much weaker than the V1 to V2 projection. It presumably represents the projection from V1 to MT (Zeki, 1976; Van Essen et al., 1981; Maunsell and Van Essen, 1983; Ungerleider and Desimone, 1986a, b). An alternative possibility is that it represents 3 separate visual areas in the superior temporal sulcus. To settle this issue, one would need to repeat the experiment, making only a single injection in V1.

To compare the patterns of proline labeling and CO staining in V2, we examined sections at higher magnification. Figure 2C shows the V2 label resulting from the middle proline injection into V1. The grayscale has been digitally inverted to simulate a lightfield view of the label. It forms a complex pattern, comprised of several large patches. Figure 2D shows the pattern of CO staining from

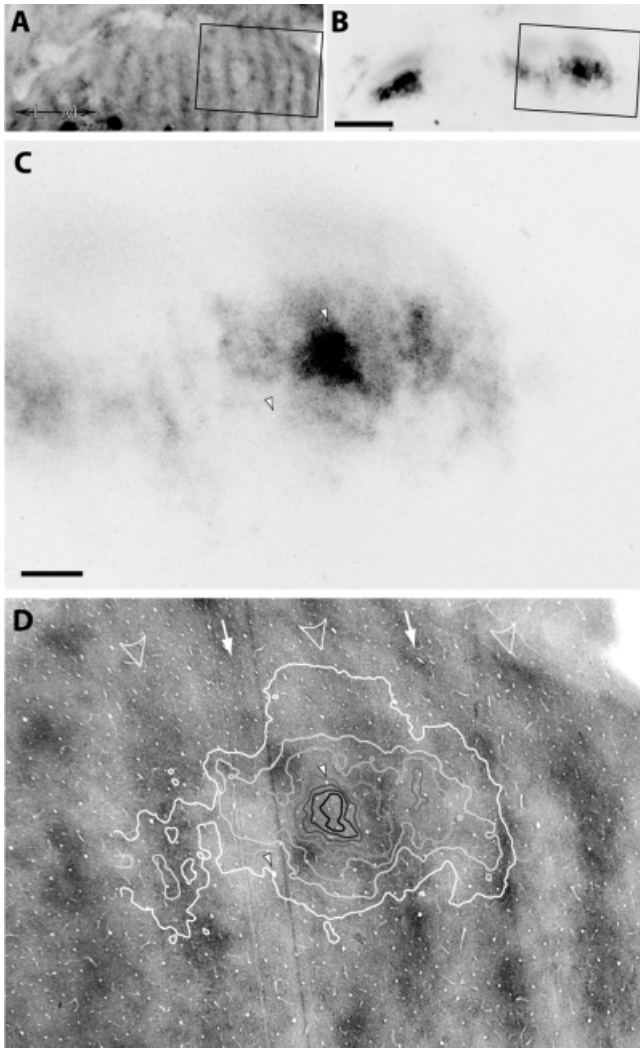


Fig. 4. Monkey 3, left hemisphere. **A:** Low magnification view of dorsal second visual area (V2) stained for cytochrome oxidase (CO). The black rectangle frames the same field in B, and is shown at higher magnification in C and D. The L-M arrow indicates the lateromedial axis in the intact brain. **B:** Autoradiograph adjacent to the CO section in A. **C:** High magnification view of the boxed region in B, centered on the medial terminal projection field. Label from a neighboring field appears in the left part of the panel. **D:** Contour plot of the label density overlaid on the CO pattern. Thin stripes are indicated by arrows and the thick stripes by open arrowheads. The two peaks of heaviest label lie in pale CO stripes, split by a band of weaker labeling in a CO thick stripe. Scale bars = 5 mm for A,B, 1 mm for C,D.

the adjacent section, passing through layer 4. There was little tissue distortion between these adjacent sections, so that nearly all of the blood vessels could be matched perfectly by simply superimposing the photographs. To compare the two images, we generated a contour plot of the density of silver grains in the [^3H]proline autoradiograph (Fig. 2E). The contour plot was then transferred onto the appropriate location in the CO section (Fig. 2F). This allows one to appreciate at a glance the relationship between proline density and CO activity.

Figure 2F illustrates two findings. First, the richest [^3H]proline label lay in the palest CO areas. There were

two peaks of label density, and both fell within pale stripes. Therefore, this projection field was rated “anti-correlated.” Second, the contour profiles followed the changes in CO density with great fidelity, as if the proline label were nestled within the pale stripes. For example, two ridges of proline label extended from the darkest peak, which was situated in a pale stripe. The “southern” ridge (Fig. 2F, blue arrow) ran through a pale breach in a thin stripe and entered a neighboring pale stripe, where it formed a second peak. The “eastern” ridge (Fig. 2F, green arrow) ran along a pale area where a thick stripe came to an end. Although all three stripe types received input from V1, the axon terminal fields in the pale CO stripes appeared to contain substantially more proline label. The contour profiles allow one to judge the difference fairly accurately. In Figure 2F, the darkest profile centered on a pale stripe was level 8, whereas the darkest profile centered on a dark stripe was level 4. Therefore, approximately twice the peak label density was present in the pale stripe.

Pale V2 stripes might be preferentially labeled by making small tracer injections into V1 centered in interpatch regions within layers 2/3 (because this V1 compartment is a source of projections to pale stripes; see Livingstone and Hubel, 1984). This would provide a trivial explanation for our findings in Figure 2. However, to avoid favoring any single stripe type, we made large injections in V1 designed to swamp the populations of cells projecting to all 3 V2 stripe types. Figure 3A is a higher power image of the autoradiograph in Figure 2B, taken with a shorter exposure. The same field has been photographed in lightfield in Figure 3B. The injections (15 μCi in 140 nl), which were the smallest made in any animal, were more than 3 mm in diameter. Figure 3C–E compares the size of the left injection with the array of CO patches. The density profile of the injection is wide enough to encompass roughly 20 CO patches and their associated interpatches. Therefore, we were assured that our injections did not selectively target interpatch regions.

Figure 4 shows an example from a different monkey, again demonstrating multiple patches of label in V2. The overall size of the projection field and the widths of the patches agree well with a previous study in macaques (Van Essen et al., 1986, see their Fig. 19). The contour plots in Figure 4 identified two peaks of proline label, split by weaker label in a thick stripe. This projection field was also rated “anti-correlated.”

Figure 5 is an example from another monkey, showing anti-correlation between CO staining and proline label. There are two peaks of [^3H]proline label, both landing on pale stripes, separated by diminished labeling in a thin stripe. This label resulted from an injection of 100 μCi [^3H]proline in 250 nl. The injections in this animal were our largest, and they produced an artifact in V2. In the intact brain, the posterior wall of the lunule sulcus lies back-to-back with dorsal V1. With big injections, the proline can diffuse through the white matter into V2 (Fig. 5E,F). In most cases, this “blow-through” artifact was offset from the labeled projection fields in V2, as seen in the medial injection in Figure 5. However, in 3 injections the “blow-through” artifact contaminated the projection field, as shown in the middle injection in Figure 5. In such cases, the injection was excluded from analysis.

The [^3H]proline which diffused into V2 was easy to differentiate from the projection fields which arose from

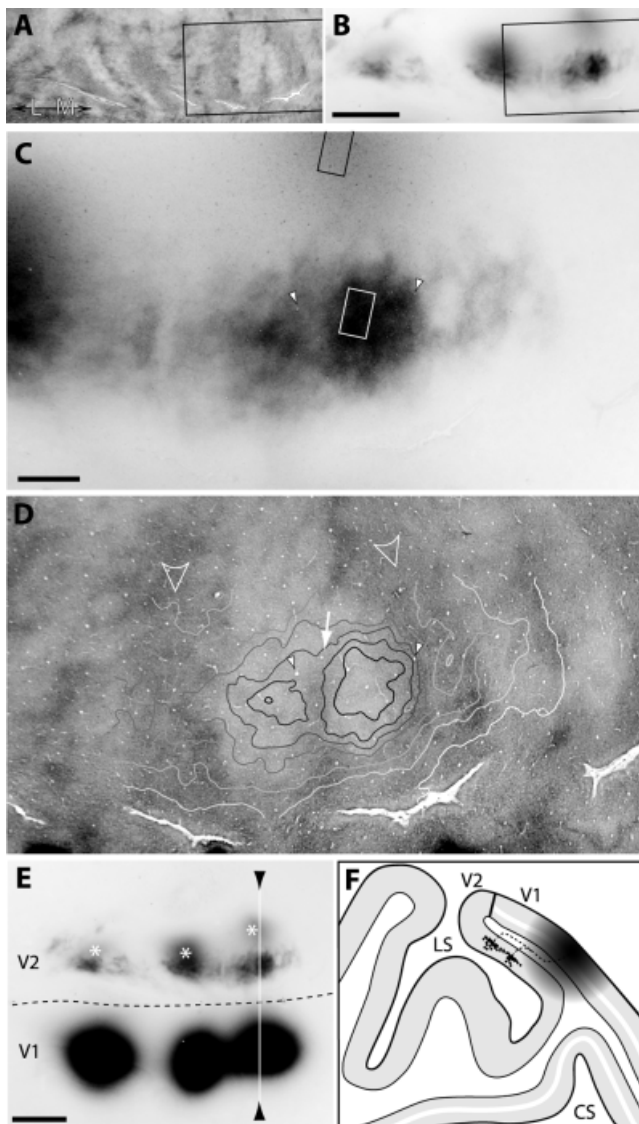


Fig. 5. Monkey 4, left hemisphere. **A:** Low magnification view of left second visual area (V2) stained for cytochrome oxidase (CO). The L-M arrow indicates the lateromedial axis. Outlined region is shown in D. **B:** Autoradiograph adjacent to A. The middle V2 projection field was obscured by diffusion of the tracer from the injection site. It was excluded from our analysis. **C:** High magnification view of the terminal primary visual cortex (V1) injection. Boxed regions are shown in Figure 6. **D:** Contour plot of the label density overlaid on the CO pattern. Two fields of heavy anterograde label are situated in the center of pale CO stripes, divided by an area of reduced labeling in a thin CO stripe (arrow). The contour lines are truncated at the upper part of the figure where proline diffused through the cortex from the injection site. Small arrowheads show blood vessels used for alignment in C,D. **E:** Autoradiograph showing the three V1 injections, their V2 projection fields, and "blow-through" diffusion artifacts (asterisks). White line indicates the slice diagrammed in F. **F:** Sagittal view showing schematically how ^3H proline can diffuse from the V1 injection site into the posterior bank of the lunate sulcus to contaminate V2. Fortunately, in most cases this leakage was clearly offset from the transport field. LS, lunate sulcus; CS, calcarine sulcus. Scale bars = 5 mm for A,B,E, 1 mm for C,D.

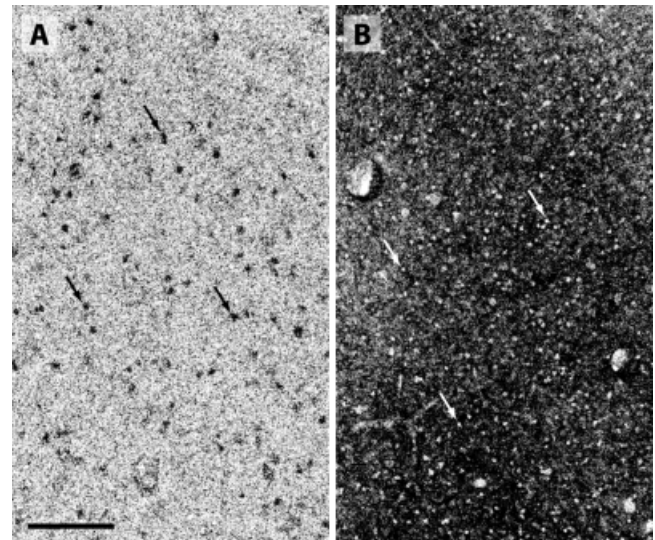


Fig. 6. **A:** Lightfield autoradiograph of the region enclosed by the black rectangle in Figure 5C, showing ^3H proline which diffused from the primary visual cortex (V1) injection site into second visual area (V2). It contains numerous dark labeled cell bodies (black arrows) which indicate local, neuronal uptake of ^3H proline. **B:** Lightfield autoradiograph of the region enclosed by the white rectangle in Figure 5C, showing ^3H proline axonally transported to the V2 projection field. Numerous unlabeled, pale cell bodies (white arrows) are outlined by labeled, dark neuropil. Autoradiographic emulsion captures the β -emission of tritium from the most superficial $\sim 5 \mu\text{m}$ of the tissue (Caviness and Barkley, 1971). The silver grains thus provide a "thin section" sample of the label. Scale bar = 100 μm for A,B.

anterograde axonal transport. First, the clouds of diffused proline were always located in V2 directly opposite the V1 injection site (before flatmounting). Second, the "blow-through" ^3H proline did not have a patchy, irregular structure typical of genuine projection fields. Instead, its density changed along a smooth gradient, as one would expect from diffusion. Third, bona fide terminal labeling was readily distinguishable from ^3H proline diffusion at higher magnification. Neurons at injection sites and in regions of diffusion artifact exhibited dense somatic labeling from incorporation of ^3H proline (Fig. 6A), whereas terminal fields showed stronger neuropil labeling with holes representing unlabeled cell bodies (Fig. 6B; Cowan et al., 1972; Hendrickson, 1972; Graybiel, 1975).

In this study, we relied principally on comparison of proline and CO in adjacent sections. Although sections can be aligned faithfully by using blood vessels, this approach is always vulnerable to the criticism that the sections might be out of register. Therefore, in each animal we double-labeled 3–5 sections for proline and CO to verify our results. The sections were reacted first for CO and photographed (Fig. 7A). The coverslip and Permount were then removed by soaking the slide in xylene. After the slide was processed for autoradiography, it was rephotographed (Fig. 7B). By using darkfield illumination and crossed polaroid filters, it was possible to photograph the silver grains without interference from the CO stain (Fig. 7C). In this example, from Monkey 1, a single peak of proline label coincided with a pale stripe (Fig. 7D). The projection field was rated "anti-correlated."

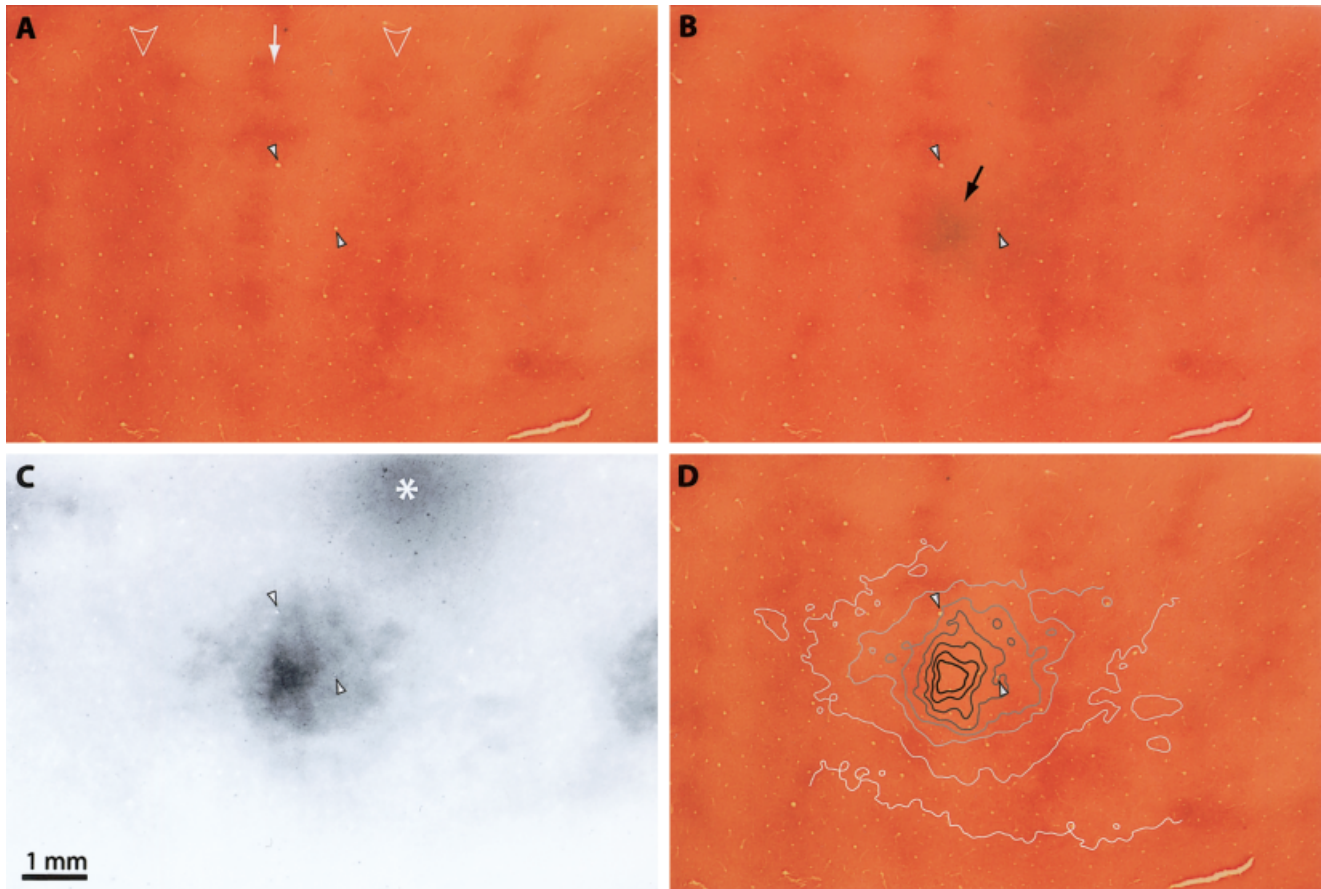


Fig. 7. Monkey 1, left hemisphere. **A:** Cytochrome oxidase (CO) section showing thick (open arrowheads) and thin (arrow) stripes in second visual area (V2). Filled arrowheads show the same blood vessels in A–D. **B:** The same field, after autoradiography, showing densest proline (black arrow) in a pale stripe. **C:** Autoradiograph of the section in B, taken in darkfield through crossed polaroid filters to

eliminate interference from the CO stain. Asterisk shows “blow-through” label, which did not contaminate the projection field. **D:** Contour plot of the $[^3\text{H}]$ proline label in C superimposed over the original CO photograph in A, confirming that the proline peak coincided with a pale stripe. Double-labeled sections eliminate the problem of section alignment. Scale bar = 1 mm for A–D.

As we have pointed out previously (Fig. 1), proline label in V2 is richest in layer 4, whereas CO density is greatest in layer 3. This discrepancy created the obvious potential for artifactual anti-correlation between CO activity and proline label. Where sections passed from layer 3 to layer 4, CO activity diminished slightly, whereas proline labeling increased. This could be misinterpreted as “stronger proline label in pale stripes.” To make sure that we were not misled by layer transitions, we examined each projection field in a series of sections cut from the pial surface to the white matter. Figure 8 compares the $[^3\text{H}]$ proline labeling to the CO pattern in 4 layers of V2. The match between the peaks of proline label and pale CO stripes was present in each layer. The densest proline label appeared in layer 4, where the CO pattern had the highest relative contrast. The proline label in layer 5/6 was quite faint, with little substructure. It presumably reflected mostly unbranched axons heading to superficial layers. The CO stripe pattern was consistent through the depth of the cortex. The same was true of the proline label: it was aligned in each layer, forming anatomical “columns” through the cortex. This assured us that the match be-

tween proline label and CO pale stripes was not an artifact of layer transitions.

Figure 9 shows an exceptional case of a laminar difference in the pattern of terminal projections between layer 2/3 and 4. In layer 4, two peaks of $[^3\text{H}]$ proline label were present. They both landed in CO pale stripes, leading us to rate the projection field as “anti-correlated.” In layers 2/3, the overall intensity of label was reduced, as expected. Surprisingly, the left peak of label was absent. Loss of this left peak showed that the distribution of label was not perfectly columnar through the cortical layers in every single case. Curiously, the left proline peak in layer 4 (Fig. 9C) was located at the far left edge of the pale stripe. To leave no retinotopic gap in the projections to pale stripes emanating from the injection site, one would have expected it to be located at the right edge. The presence of this gap suggests that there are other factors besides retinotopy and stripe type that shape the projections from V1 to V2.

The original reports of the V2 CO stripes emphasized that they contain subregions of variable density. The stripes have been described as “a complicated pattern

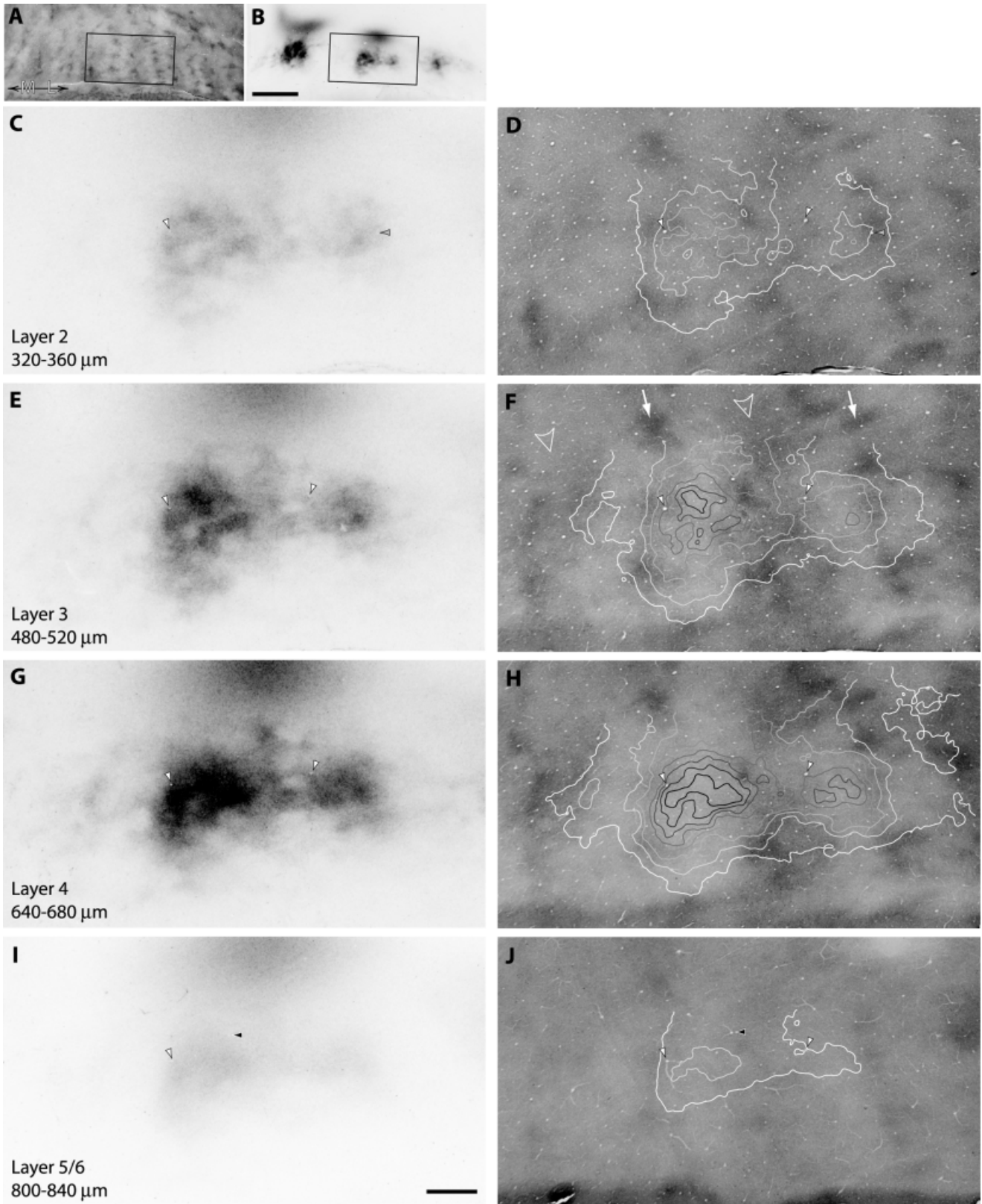


Fig. 8. Monkey 1, right hemisphere. **A:** Low power view of second visual area (V2) stained for cytochrome oxidase (CO). The black rectangle frames the region shown below at higher power in different cortical layers. **B:** Autoradiograph adjacent to the CO section in A. Left column (**C,E,G,I**): Autoradiographs taken through layers 2–6 in V2; white matter was reached at a depth of 1,040 μm . The sections were photographed with identical exposures to illustrate the relative density of [^3H]proline label. Various arrowheads point to blood vessels

used for alignment in C–J. Right column (**D,F,H,J**): CO sections directly underneath those in the left column. Photographs were taken with identical exposures and contrast-enhanced to the same degree. Contour plots in all panels were scaled relative to the density of proline label in G. In F, open arrowheads point to thick stripes and arrows to thin stripes. The heaviest proline appeared in pale stripes, regardless of cortical layer. This projection field had 2 peaks and was rated “anti-correlated.” Scale bars = 5 mm for A,B, 1 mm for C–J.

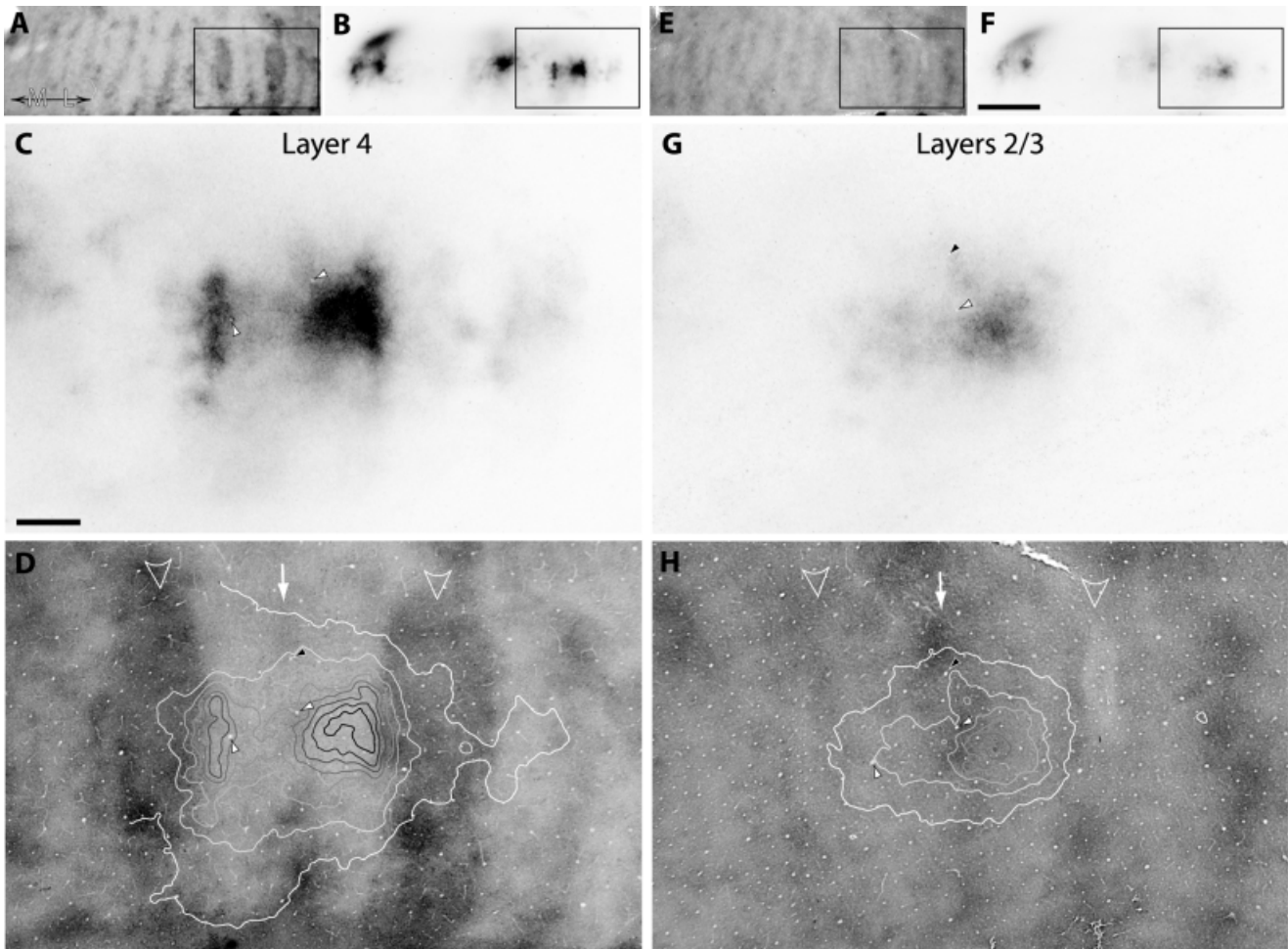


Fig. 9. Monkey 3, right hemisphere. Left side (A–D): Layer 4 contained 2 peaks of [^3H]proline label, each located in a pale stripe. The proline label in the left pale stripe formed a ridge along the left edge of the stripe. Box in A,B,E,F is the same field shown in C,D,G,H. Right side (E–H): Layers 2/3 had less proline label than layer 4, and only one peak. The second, left peak was absent. This case was

unusual, because the pattern of proline labeling was similar from layer to layer in all other second visual area (V2) projection fields. Filled arrowheads show blood vessels used for alignment. In D,H, open arrowheads point to thick stripes and arrows to thin stripes. Scale bars = 5 mm for A,B,E,F, 1 mm for C,D,G,H.

consisting of small, irregular fluctuations in density of cytochrome oxidase" (Horton, 1984, p. 213), "irregular and discontinuous, consisting of dark clumps separated by narrow isthmuses" (Hubel and Livingstone, 1987, p. 3404), or "a string of patches" (Tootell and Hamilton, 1989, p. 2641). In many projection fields, the proline label fluctuated on a fine scale with the local CO activity, but in opposing contrast. Figure 10 shows that within each stripe type, wherever CO is locally darker, the proline label is relatively lighter, and vice versa. This suggests that the fine mottling seen in the CO staining of V2 stripes often bears a close relationship to the strength of V1 input.

Table 1 summarizes the results of this study. Of 34 injections, 32 were examined in flatmounts, lending themselves to analysis. Three were obscured by "blow-through" artifact, leaving a total of 29 usable injections. In the majority (21/29), proline label was anti-correlated with CO density. However, 7/29 projection fields were classified as "uncorrelated," meaning that peaks of proline fell over both pale and darks CO stripes. Figure 11 shows a typical

example of an "uncorrelated" projection field. There were three peaks of proline label. The middle peak coincided with a thick stripe, although the two flanking peaks matched pale stripes. A single example (1/29) was found of a correlated projection field (Fig. 12A–D). There were 3 proline peaks, hitting a thin stripe and two thick stripes. Figure 12E–H shows a separate injection in this hemisphere with enriched pale stripe labeling, underscoring that the correlated projection field was genuinely exceptional, even in this animal.

DISCUSSION

More than 20 years ago, it was discovered that V2 receives patchy projections from V1 (Rockland and Pandya, 1979; Wong-Riley, 1979b; Lund et al., 1981). This phenomenon seems to be common in sensory areas, because it is also found between primary and secondary areas of the auditory and somatosensory cortices (Jones et al., 1978; Fitzpatrick and Imig, 1980). The patchy

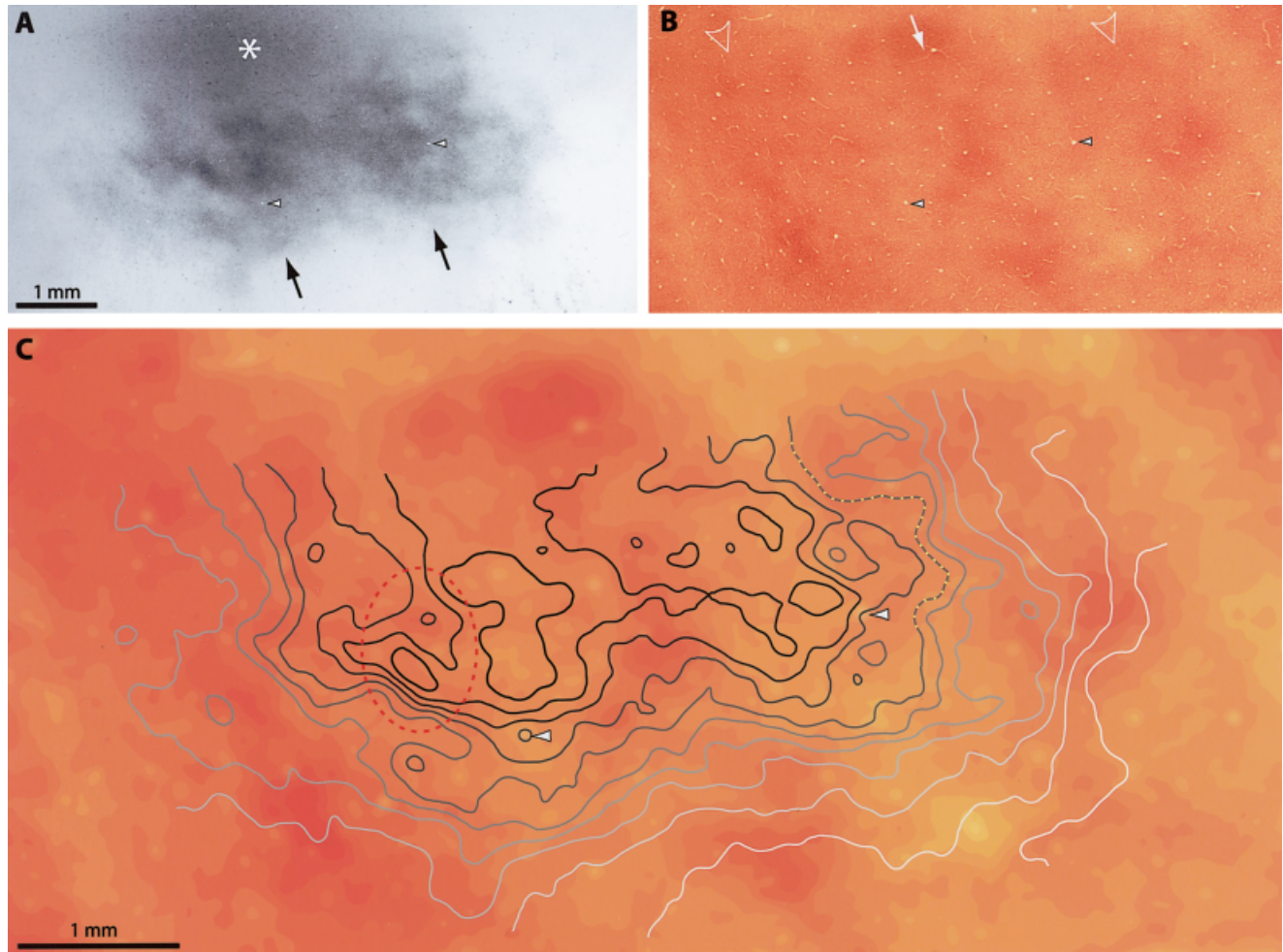


Fig. 10. Monkey 4, right hemisphere. **A:** Autoradiograph of a terminal field in layer 4, containing a complex pattern of label in 2 main fields (black arrows). There is some "blow-through" label marked with an asterisk just above the projection zone. Filled arrowheads show same blood vessels in A–C. **B:** More superficial section, in upper layer 4, stained for cytochrome oxidase (CO). White arrow indicates a thin stripe, open arrowheads 2 thick stripes. **C:** Contour plot of [^3H]proline labeling aligned over a filled-contour plot of the CO pattern. The 2 major fields of

proline label coincided with 2 pale CO stripes, flanking a thin stripe, making this projection field "anti-correlated." Even within the second visual area (V2) stripes, the [^3H]proline label became locally denser wherever the CO was locally paler (an example is circled with a dashed red line). Often a proline contour line followed a course along a V2 stripe which mimicked the CO contour, like a road following the topography of a mountainside (for example, the segment of contour marked with yellow dots). Scale bars = 1 mm for A–C.

TABLE 1. Summary of V1 Projection Fields and Their Correlation With Cytochrome Oxidase Activity in V2¹

Animal	Injection size	Left hemisphere injections			Right hemisphere injections		
		Medial	Middle	Lateral	Medial	Middle	Lateral
Monkey 1 (dorsal)	15 $\mu\text{Ci}/140$ nl	Uncorrelated (Fig. 11)	Anti-correlated (Fig. 7)	Uncorrelated	Anti-correlated	Anti-correlated (Fig. 8)	Anti-correlated
Monkey 1 (ventral)	15 $\mu\text{Ci}/140$ nl		(Not flattened) (Fig. 1)		Anti-correlated	—	Anti-correlated
Monkey 2	15 $\mu\text{Ci}/140$ nl	Anti-correlated	Anti-correlated	Anti-correlated	Anti-correlated	Anti-correlated (Fig. 2)	Anti-correlated
Monkey 3	10–20 $\mu\text{Ci}/75$ –140 nl	Anti-correlated (Fig. 4)	Uncorrelated	Uncorrelated	Anti-correlated	Anti-correlated	Anti-correlated (Fig. 9)
Monkey 4	100 $\mu\text{Ci}/250$ nl	Anti-correlated	(Artifact)	Anti-correlated (Fig. 5)	(Artifact)	(Artifact)	Anti-correlated (Fig. 10)
Monkey 5	17–56 $\mu\text{Ci}/280$ nl	Anti-correlated (Fig. 12G)	Uncorrelated	Correlated (Fig. 12C)	Anti-correlated	Uncorrelated	Uncorrelated

¹V1, V2, primary and secondary visual cortex, respectively.

projection pattern from V1 to V2 has never been compared systematically to the prominent pattern of CO stripes in V2 (Tootell et al., 1983; Horton, 1984). Fol-

lowing large V1 injections of [^3H]proline, an anterograde tracer, we found that the density of labeled axon terminals in V2 was usually related inversely to the

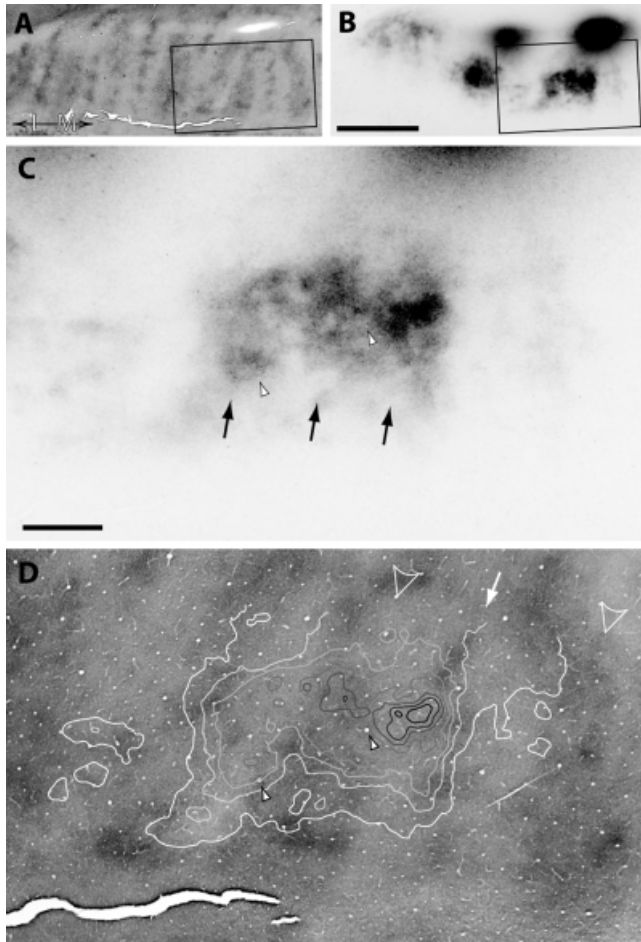


Fig. 11. Monkey 1, left hemisphere. Layer 4 of second visual area (V2) reacted for cytochrome oxidase (CO; **A**) and processed for autoradiography (**B**). **C**: High magnification view of the medial terminal projection field (outlined in **B**), showing 3 peaks marked with black arrows. Filled arrowheads point to matching vessels in **C**–**D**. **D**: The middle proline peak fell on a thick stripe (open arrowhead), whereas the two flanking proline peaks were located in pale stripes. The right proline peak, which was the densest, also extended into a thin stripe (white arrow). This projection field was rated as “uncorrelated.” Scale bars = 5 mm for **A**, **B**, 1 mm for **C**, **D**.

density of CO. In the majority of cases, pale CO stripes received the richest projection. It was often twice as dense as the projection to flanking dark stripes. There was no obvious difference in the density of projections received by thick and thin stripes. In many instances, the inverse relationship between CO level and proline terminal labeling showed a high degree of fidelity. Even within stripes, the density of CO activity often fluctuated in exact but opposite contrast to the density of proline label.

To convey the main result of this paper, namely, that projections from V1 are concentrated in pale stripes of V2, we have relied on two approaches. First, we have shown many examples (10 cases) of our raw data, illustrating at least one projection field from each animal (Table 1). Second, we have devised a system for plotting proline density as a series of topographic contours. These contour plots

allow one to determine objectively peaks of label density. The contour plots can then be superimposed on the V2 CO stripes in adjacent flatmounts for comparison. In 21/29 cases, peaks of proline label matched V2 pale stripes (Table 1). In 7/29 cases, the results were mixed, with peaks landing on pale and dark stripes. In only 1 case, all 3 proline peaks coincided with dark stripes. These data indicate that the majority of V1’s cortical output is conveyed to pale stripes, and ultimately, to extrastriate areas that receive pale stripe output (DeYoe and Van Essen, 1985; Shipp and Zeki, 1985).

There are several ways that technical errors might have led artifactually to these results. If our injections had been small, and confined to interpatches located in layers 2/3, they might have been expected to label pale stripes preferentially (Livingstone and Hubel, 1984). However, recent work (Sincich and Horton, 2002) has shown that projections to pale stripes and to thick stripes arise from the same V1 compartments: interpatches in layers 4B and 2/3. Therefore, biased placement of our injections into interpatches, or into layers 2/3 rather than layer 4B, could not explain why we obtained stronger labeling in V2 pale stripes. Moreover, to avoid favoring a single source of V1 projections, we made large injections to flood all compartments in V1 that project to V2. In fact, the injections were often large enough to contaminate V2, by diffusing through the white matter into V2 lining the lunate sulcus. In Figures 5 and 6, we show that this “blow-through” artifact did not hamper the interpretation of our data. There was also potential for artifact arising from differences in proline and CO density in different cortical layers. Proline label was heaviest in layer 4, whereas CO activity was strongest in layer 3. Thus, a flatmount section grazing the border between layers 3 and 4 might show anti-correlation between proline and CO simply on the basis of this layer transition. To eliminate this possibility, we compared proline and CO in a series of sections passing through multiple cortical layers (Fig. 8) to verify in each case that the labels were truly anti-correlated. Finally, comparison of different labels in adjacent sections is never ideal. Therefore, double-labeled sections were also examined in every hemisphere of every animal (Fig. 7).

It is noteworthy that in 8/29 cases (7 uncorrelated, plus 1 correlated), our proline injections produced strong label in dark stripes. Why did strong dark stripe label occur in these cases? The strongest labeling in V2 might be expected directly opposite an injection site in V1, because retinotopy is mirrored across the V1/V2 border. For example, if a V1 injection were centered just across from a dark V2 stripe, one might expect strongest label in that same dark stripe. To examine this point, we checked the injection site location in all 29 cases. There was no relationship between the center of an injection site, the identity (dark versus pale) of the closest stripe type, and the pattern of strongest stripe labeling. Admittedly, this analysis was tenuous, because the injections were large compared with the width of individual V2 stripes, and the most direct line to the V1/V2 border did not necessarily follow an isoecentricity contour. A stronger argument can be made by invoking the laws of probability. It seems highly unlikely that only a few of our injections were situated opposite dark stripes, given that they account for at least half the perimeter of V2. Therefore, we do not believe that weaker labeling of dark stripes in this study occurred as a result of biased placement of injections opposite pale stripes.

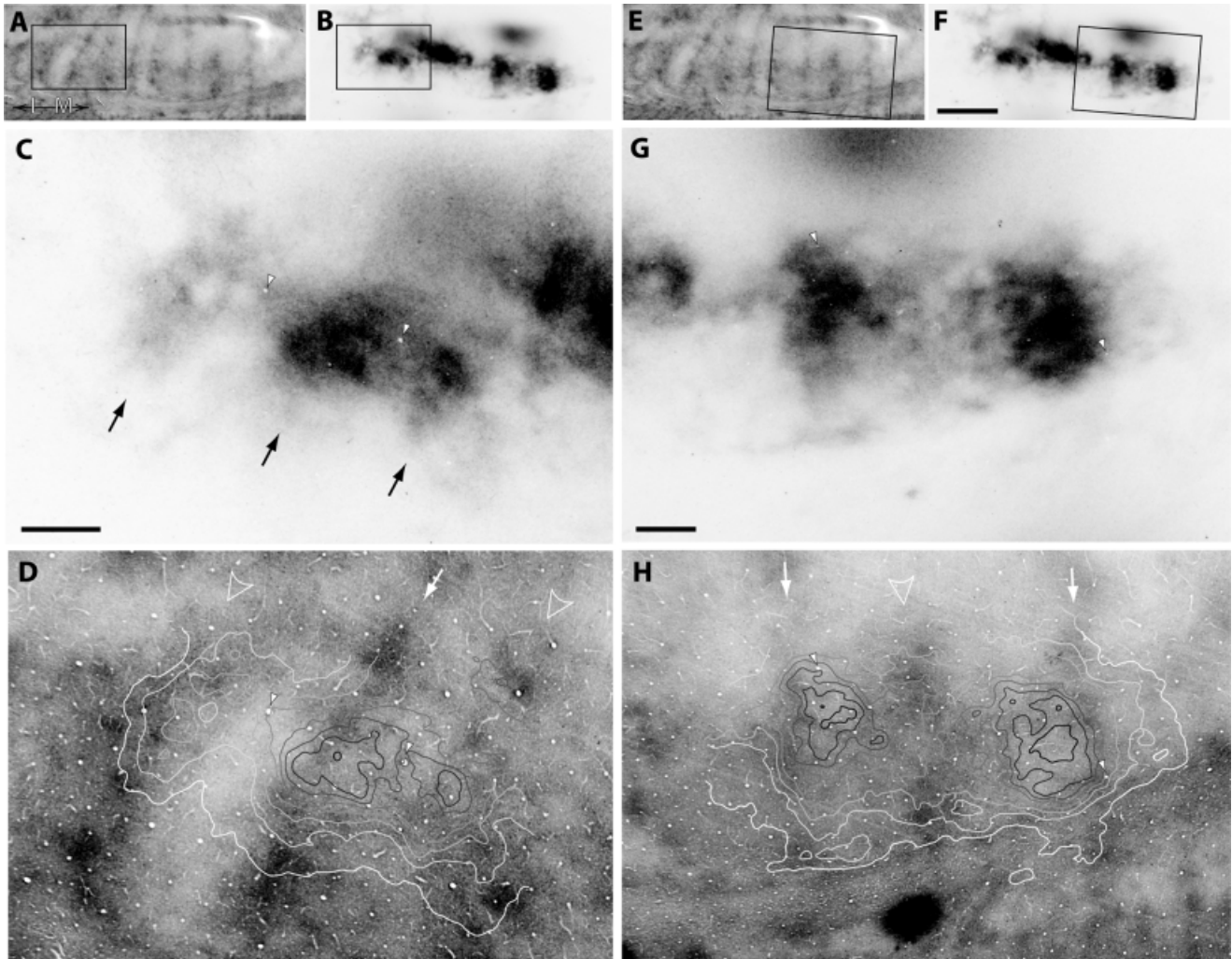


Fig. 12. Monkey 5, left hemisphere. Left column (A-D): The lateral injection in this hemisphere produced 3 peaks (black arrows) of [^3H]proline label (the label at the far right edge of panel C is from the middle injection). All 3 peaks coincided with dark cytochrome oxidase (CO) stripes (although they favored lighter regions within these dark stripes). Thus, the projection field was rated as "correlated." Thick stripes are shown by open arrowheads, thin by arrows in D,H. It was the only case of a primary visual cortex (V1) injection producing label

that always peaked in dark stripes. Right column (E-H): Anti-correlated projection field, containing two peaks of proline label centered on pale stripes. This anti-correlated projection field was from the same section as the correlated projection field in the left column, showing that both projection patterns can exist in the same animal. Boxed areas in A,B,E,F are enlarged in C,D,G,H. Matching blood vessels are indicated by filled arrowheads in C,D and G,H. Scale bars = 5 mm for A,B,E,F, 1 mm for C,D,G,H.

Pale, thin, and thick stripes have been reported to contain separate retinotopic maps (Roe and Ts'o, 1995, 1997; Ts'o et al., 2001). These maps may be interleaved in a discontinuous fashion, with jumps in retinotopic position at stripe borders. If an injection were placed opposite a pale stripe, the V2 label would be fractured into multiple patches corresponding to breaks in the retinotopic map (Fig. 13A). Pale stripes occur at twice the frequency of thin stripes or thick stripes. As a result, only part of a dark stripe between two labeled pale stripes would be filled, creating a tendency for proline label to be centered on pale stripes. Such labeling patterns were seen in some cases (for example, Fig. 4), providing indirect support for the Roe and Ts'o (1995, 1997) scheme of V2 retinotopy. However, there are several reasons why we do not believe that fractures in the V2 retinotopic map account for our re-

sults. First, note that injections directly opposite thick or thin dark stripes (Fig. 13B) should produce no patches in V2, yet patches were seen after almost every V1 injection. Second, as argued in the previous paragraph, it would be unlikely for the majority of our injections to fall opposite pale stripes by chance. Third, the V2 proline label showed an allegiance for pale stripes that far surpassed the affinity predicted by the model in Figure 13.

Given our results, it is natural to inquire whether pale stripes receive input from a disproportionate fraction of V1 projecting neurons. There are no quantitative data addressing this issue. Taking their surface area as a guide, CO patches occupy perhaps one-third of striate cortex. Any more precise figure suffers from being criterion-dependent (Purves and LaMantia, 1993; Farias et al., 1997). If patches occupy one-third of striate cortex,

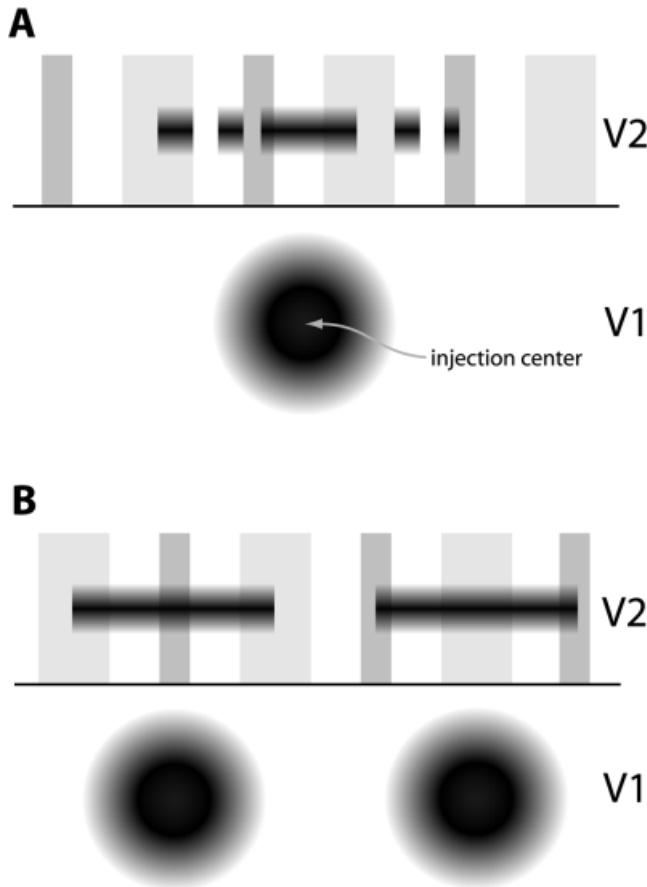


Fig. 13. **A:** Prediction of labeling pattern in second visual area (V2) from a primary visual cortex (V1) proline injection situated opposite a pale stripe. If V2 contains separate retinotopic maps for each stripe type, the proline label will be separated by fractures, resulting in several patches of label located in pale stripes. This occurs because there are twice as many pale stripes as thin or thick stripes. **B:** Prediction of labeling pattern from a V1 injection made exactly opposite a thin (left) or thick (right) stripe. In these cases, there would be continuous label in V2.

only half as many neurons project to thin stripes compared to pale stripes (assuming that equal proportions of neurons in patches and interpatches project to V2). However, this 1:2 ratio would not give rise to a denser projection to pale stripes, because there are two pale stripes for each thin stripe, which would equalize the input.

It is possible that axons projecting to pale stripes have more extensive terminal arbors, resulting in a greater density of synaptic contacts. Single V1-to-V2 axons have been reconstructed in the macaque, but not correlated with V2 stripe type (Rockland and Virga, 1990). With few exceptions, the terminal cluster volumes and bouton counts form a unimodal population, varying in size by a factor of ~ 4 . Our data suggest that the more elaborate, synapse-dense arbors predominate in the pale CO stripes.

Contrary to our original expectation, the darkest regions of CO staining in V2 did not coincide with maximum V1 input. Layer 4, which receives the richest input from V1, did not contain the strongest CO activity. More strikingly, the dark stripes got less input from V1 than the pale

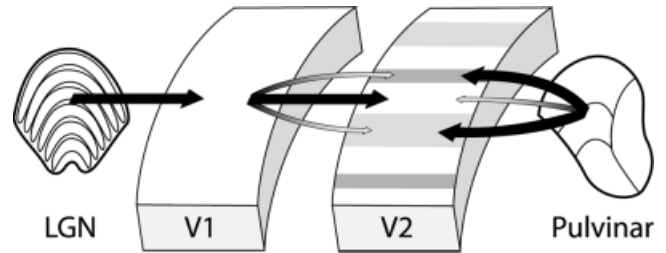


Fig. 14. Schematic diagram showing how projections from primary visual cortex (V1) and the pulvinal converge in second visual area (V2). As indicated by black arrows, the projections from V1 are richest to pale stripes, whereas those from the pulvinal are strongest to thick and thin stripes. The segregation is far from absolute, as shown by gray arrows indicating weaker projections. The strongest projections from V1 and the pulvinal are interdigitated in V2. LGN, lateral geniculate nucleus.

stripes. This finding suggests that the V2 pattern of CO activity is not a simple reflection of the excitatory drive imparted by V1. Rather, it appears that the dominant CO pattern in V2 is due to an interplay between other inputs and outputs. The V2 stripes differ in terms of their relative input from V1, from the pulvinal, and in terms of their output to area V4 and V5 (DeYoe and Van Essen, 1985; Shipp and Zeki, 1985).

The pulvinal provides the major thalamic input to V2 (Ferrier and Turner, 1898; Le Gros Clark and Northfield, 1937; Chow, 1950; Benevento and Rezak, 1976; Trojanowski and Jacobson, 1976; Ogren and Hendrickson, 1977; Lund et al., 1981; Kennedy and Bullier, 1985; Adams et al., 2000). The pulvinal efferents to V2 are highly correlated with CO stripe type (Livingstone and Hubel, 1982; Levitt et al., 1995). The thin stripes and the thick stripes get much stronger pulvinal input than the pale stripes. Moreover, the input terminates predominately in layer 3, the V2 layer with strongest CO activity. By contrast, V1 input is richest to pale stripes, and to layer 4. Thus, the V1 and pulvinal inputs to V2 are interleaved, as illustrated in Figure 14, in terms of both CO stripe type and cortical layer.

V2 is the first site in the cortex for convergence of the retino-geniculo-cortical pathway and the retino-pulvino-cortical pathway. An important function of V2 may be to integrate visual information emanating from these two visual streams. It would be vital to learn how inputs from V1 and the pulvinal are combined in V2. Given that the inputs favor different stripe types, it seems likely that they target separate populations of neurons. Although V1 and pulvinal inputs may be segregated to some degree, there is an extensive network in layers 2/3 of local projections that runs between different stripe types (Rockland, 1985; Levitt et al., 1994; Malach et al., 1994). Input of visual information from V1 and attentional signals from the pulvinal (Robinson and Cowie, 1997; Grieve et al., 2000) could be blended in V2 via this network of intracortical connections.

ACKNOWLEDGMENTS

This work was supported by grants R01-EY10217 (J.C.H.) and F32-EY13676 (L.C.S.) from the National Eye Institute. The Beckman Vision Center is supported by

core grant P30-EY02162 from the National Eye Institute. Support was also received from That Man May See, Inc. and Research to Prevent Blindness (Lew R. Wasserman Merit Award to J.C.H.). We thank Davina Hocking for her excellent help with tissue processing. We thank Daniel Adams and Antonella Antonini for their independent rating of the projection fields. We thank Julie Schnapf and Daniel Adams for their comments on the manuscript.

LITERATURE CITED

- Adams MM, Hof PR, Gattass R, Webster MJ, Ungerleider LG. 2000. Visual cortical projections and chemoarchitecture of macaque monkey pulvinar. *J Comp Neurol* 419:377–393.
- Beck PD, Kaas JH. 1999. Cortical connections of the dorsomedial visual area in old world macaque monkeys. *J Comp Neurol* 406:487–502.
- Benevento LA, Rezak M. 1976. The cortical projections of the inferior pulvinar and adjacent lateral pulvinar in the rhesus monkey (*Macaca mulatta*): an autoradiographic study. *Brain Res* 108:1–24.
- Burkhalter A, Felleman DJ, Newsome WT, Van Essen DC. 1986. Anatomical and physiological asymmetries related to visual areas V3 and VP in macaque extrastriate cortex. *Vision Res* 26:63–80.
- Caviness VS, Barkley DS. 1971. Section thickness and grain count variation in tritium autoradiography. *Stain Technol* 46:131–135.
- Chow KL. 1950. A retrograde cell degeneration study of the cortical projection field of the pulvinar in the monkey. *J Comp Neurol* 93:313–340.
- Cowan WM, Gottlieb DI, Hendrickson AE, Price JL, Woolsey TA. 1972. The autoradiographic demonstration of axonal connections in the central nervous system. *Brain Res* 37:21–51.
- Cragg BG. 1969. The topography of the afferent projections in the circumstriate visual cortex of the monkey studied by the Nauta method. *Vision Res* 9:733–747.
- Crawford MLJ, Chodosh J. 1990. Cytochrome oxidase patterns in V2 cortex of macaque. *Invest Ophthalmol Visual Sci* 31:89.
- DeYoe EA, Van Essen DC. 1985. Segregation of efferent connections and receptive field properties in visual area V2 of the macaque. *Nature* 317:58–61.
- Ding Y, Casagrande VA. 1997. The distribution and morphology of LGN K pathway axons within the layers and CO blobs of owl monkey V1. *Visual Neurosci* 14:691–704.
- Farias MF, Gattass R, Piñón MC, Ungerleider LG. 1997. Tangential distribution of cytochrome oxidase-rich blobs in the primary visual cortex of macaque monkeys. *J Comp Neurol* 386:217–228.
- Felleman DJ, Burkhalter A, Van Essen DC. 1997. Cortical connections of areas V3 and VP of macaque monkey extrastriate visual cortex. *J Comp Neurol* 379:21–47.
- Ferrier D, Turner WA. 1898. An experimental research upon cerebrocortical afferent and efferent tracts. *Phil Trans Roy Soc London. Series B: Biol Sci* 190:1–44.
- Fitzpatrick KA, Imig TJ. 1980. Auditory cortico-cortical connections in the owl monkey. *J Comp Neurol* 192:589–610.
- Gattass R, Sousa APB, Gross CG. 1988. Visuotopic organization and extent of V3 and V4 of the macaque. *J Neurosci* 8:1831–1845.
- Graybiel AM. 1975. Wallerian degeneration and anterograde tracer methods. In: Cowan WM, Cuenod M, editors. *The use of axonal transport for studies of neuronal connectivity*. Amsterdam: Elsevier. p 173–216.
- Grieve KL, Acuña C, Cudeiro J. 2000. The primate pulvinar nuclei: vision and action. *Trends Neurosci* 23:35–39.
- Hendrickson AE. 1972. Electron microscopic distribution of axoplasmic transport. *J Comp Neurol* 144:381–398.
- Hendry SH, Yoshioka T. 1994. A neurochemically distinct third channel in the macaque dorsal lateral geniculate nucleus. *Science* 264:575–577.
- Horton JC. 1984. Cytochrome oxidase patches: a new cytoarchitectonic feature of monkey visual cortex. *Phil Trans Roy Soc London. Series B: Biol Sci* 304:199–253.
- Horton JC, Hocking DR. 1996. An adult-like pattern of ocular dominance columns in striate cortex of newborn monkeys prior to visual experience. *J Neurosci* 16:1791–1807.
- Hubel DH, Livingstone MS. 1987. Segregation of form, color, and stereopsis in primate area 18. *J Neurosci* 7:3378–3415.
- Jones EG, Coulter JD, Hendry SHC. 1978. Intracortical connectivity of architectonic fields in the somatic sensory, motor and parietal cortex of monkeys. *J Comp Neurol* 181:291–343.
- Kennedy H, Bullier J. 1985. A double-labeling investigation of the afferent connectivity to cortical areas V1 and V2 of the macaque monkey. *J Neurosci* 5:2815–2830.
- Kuypers HGJM, Szwarcbart MK, Mishkin M, Rosvold HE. 1965. Occipito-temporal corticocortical connections in the rhesus monkey. *Exp Neurol* 11:245–262.
- Le Gros Clark WE, Northfield DWC. 1937. The cortical projection of the pulvinar in the macaque monkey. *Brain* 60:126–142.
- Levitt JB, Yoshioka T, Lund JS. 1994. Intrinsic cortical connections in macaque visual area V2: evidence for interaction between different functional streams. *J Comp Neurol* 342:551–570.
- Levitt JB, Yoshioka T, Lund JS. 1995. Connections between the pulvinar complex and cytochrome oxidase-defined compartments in visual area V2 of macaque monkey. *Exp Brain Res* 104:419–430.
- Livingstone MS, Hubel DH. 1982. Thalamic inputs to cytochrome oxidase-rich regions in monkey visual cortex. *Proc Natl Acad Sci USA* 79:6098–6101.
- Livingstone MS, Hubel DH. 1984. Anatomy and physiology of a color system in the primate visual cortex. *J Neurosci* 4:309–356.
- Lund JS, Hendrickson AE, Ogren MP, Tobin EA. 1981. Anatomical organization of primate visual cortex area VII. *J Comp Neurol* 202:19–45.
- Malach R, Tootell RB, Malonek D. 1994. Relationship between orientation domains, cytochrome oxidase stripes, and intrinsic horizontal connections in squirrel monkey area V2. *Cereb Cortex* 4:151–165.
- Martinez-Millán L, Holländer H. 1975. Cortico-cortical projections from striate cortex of the squirrel monkey (*Saimiri sciureus*). A radioautographic study. *Brain Res* 83:405–417.
- Maunsell JH, Van Essen DC. 1983. The connections of the middle temporal visual area (MT) and their relationship to a cortical hierarchy in the macaque monkey. *J Neurosci* 3:2563–2586.
- Maunsell JHR, Newsome WT, Van Essen DC. 1980. The spatial organization of connections between V1 and V2 in the macaque: patchy and non-patchy projections. *Soc Neurosci Abstr* 6:580.
- Mettler FA. 1935. Corticofugal fiber connections of the cortex of *Macaca mulatta*: the occipital region. *J Comp Neurol* 61:221–256.
- Ogren MP, Hendrickson AE. 1977. The distribution of pulvinar terminals in visual areas 17 and 18 of the monkey. *Brain Res* 137:343–350.
- Olavarria JF, Van Essen DC. 1997. The global pattern of cytochrome oxidase stripes in visual area V2 of the macaque monkey. *Cereb Cortex* 7:395–404.
- Olavarria JF, Van Sluyters RC. 1985. Unfolding and flattening the cortex of gyrencephalic brains. *J Neurosci Methods* 15:191–202.
- Poliak SL. 1932. The main afferent fiber systems of the cerebral cortex in primates: an investigation of the central portions of the somatosensory, auditory and visual paths of the cerebral cortex. Berkeley: University of California Press.
- Purves D, LaMantia A. 1993. Development of blobs in the visual cortex of macaques. *J Comp Neurol* 334:169–175.
- Robinson DL, Cowie RJ. 1997. The primate pulvinar: structural, functional, and behavioral components of visual salience. In: Steriade M, Jones EG, McCormick DA, editors. *Thalamus*. Oxford: Elsevier. p 53–92.
- Rockland KS. 1985. A reticular pattern of intrinsic connections in primate area V2 (area 18). *J Comp Neurol* 235:467–478.
- Rockland KS, Pandya DN. 1979. Laminar origins and terminations of cortical connections of the occipital lobe in the rhesus monkey. *Brain Res* 179:3–20.
- Rockland KS, Virga A. 1990. Organization of individual cortical axons projecting from area V1 (area 17) to V2 (area 18) in the macaque monkey. *Visual Neurosci* 4:11–28.
- Roe AW, Ts'o DY. 1995. Visual topography in primate V2: multiple representation across functional stripes. *J Neurosci* 15:3689–3715.
- Roe AW, Ts'o DY. 1997. The functional architecture of Area V2 in the macaque monkey. In: Rockland KS, Kaas JH, Peters A, editors. *Cerebral cortex*. New York: Plenum Press. p 295–333.
- Shipp S, Zeki S. 1985. Segregation of pathways leading from area V2 to areas V4 and V5 of macaque monkey visual cortex. *Nature* 315:322–325.
- Sincich LC, Horton JC. 2002. Divided by cytochrome oxidase: A map of the projections from V1 to V2 in macaques. *Science* (in press).
- Tootell RB, Silverman MS. 1985. Two methods for flat-mounting cortical tissue. *J Neurosci Methods* 15:177–190.
- Tootell RBH, Hamilton SL. 1989. Functional anatomy of the second visual area (V2) in the macaque. *J Neurosci* 9:2620–2644.

- Tootell RBH, Silverman MS, De Valois RL, Jacobs GH. 1983. Functional organization of the second cortical visual area in primates. *Science* 220:737–739.
- Trojanowski JQ, Jacobson S. 1976. Areal and laminar distribution of some pulvinar cortical efferents in rhesus monkey. *J Comp Neurol* 169:371–392.
- Ts'o DY, Roe AW, Gilbert CD. 2001. A hierarchy of the functional organization for color, form and disparity in primate visual area V2. *Vision Res* 41:1333–1349.
- Ungerleider LG, Desimone R. 1986a. Cortical connections of visual area MT in the macaque. *J Comp Neurol*:190–222.
- Ungerleider LG, Desimone R. 1986b. Projections to the superior temporal sulcus from the central and peripheral field representations of V1 and V2. *J Comp Neurol* 248:147–163.
- Van Essen DC, Zeki SM. 1978. The topographic organization of rhesus monkey prestriate cortex. *J Physiol* 277:193–226.
- Van Essen DC, Maunsell JHR, Bixby JL. 1981. The middle temporal visual area in the macaque: myeloarchitecture, connections, functional properties and topographic organization. *J Comp Neurol* 199:293–326.
- Van Essen DC, Newsome WT, Maunsell JH, Bixby JL. 1986. The projections from striate cortex (V1) to areas V2 and V3 in the macaque monkey: asymmetries, areal boundaries, and patchy connections. *J Comp Neurol* 244:451–480.
- Weller RE, Kaas JH. 1983. Retinotopic patterns of connections of area 17 with visual areas V-II and MT in macaque monkeys. *J Comp Neurol* 220:253–279.
- Wong-Riley MTT. 1979a. Changes in the visual system of monocularly sutured or enucleated cats demonstrable with cytochrome oxidase histochemistry. *Brain Res* 171:11–28.
- Wong-Riley MTT. 1979b. Columnar cortico-cortical interconnections within the visual system of the squirrel and macaque monkeys. *Brain Res* 162:201–217.
- Zeki SM. 1969. Representation of central visual fields in prestriate cortex of monkey. *Brain Res* 14:271–291.
- Zeki SM. 1976. The projections to the superior temporal sulcus from areas 17 and 18 in the rhesus monkey. *Proc Roy Soc London. Series B: Biol Sci* 193:199–207.
- Zeki SM. 1978. The third visual complex of rhesus monkey prestriate cortex. *J Physiol* 277:245–272.